CHEMISTRY
A EUROPEAN JOURNAL

DOI: 10.1002/chem.200902664

A Series of Open-Framework Aluminoborates Templated by Transition-Metal Complexes

Jian Zhou,[a, c] Wei-Hui Fang,[a] Cheng Rong,[a] and Guo-Yu Yang*[a, b]

Abstract: A series of open-framework aluminoborates (ABOs) $[M(dien)_2][AlB_6O_{11}(OH)]$ (M = Co (**Ia**), Ni (**Ib**), Cd (**Ic**), Zn (**Id**); dien = diethylenetriamine) and $[M(en)_3][AlB_7O_{12}(OH)_2]\cdot(H_2O)_{0.25}$ (M = Co (**IIa**), Ni (**IIb**); en = ethylenediamine) have been made under hydrothermal conditions and characterized by elemental analysis, IR spectroscopy, thermogravimetric analysis, UV/Vis and fluorescence spectroscopy, powder X-ray diffraction, single-crystal X-ray diffraction, and nonlinear optical determination. These compounds were classified as two structural types: Type **I** (**Ia–d**) contains AlO_4 tetrahedra and $B_6O_{11}(OH)$ clusters, which link to form a new 3D framework with 7-/9-ring helical channels and large 13-ring channels; whereas type **II** (**IIa**,**b**) is composed of AlO_4 tetrahedra, chain-like $B_4O_6(OH)_2$ tetramer, and crablike B_6O_{12} clusters, which interconnect to form other new 3D frameworks with 8-ring helical channels, rare 16-ring double-helical channels, and larger odd 15-ring channels. These compounds represent the first examples of 3D ABOs templated by transition-metal complexes (TMCs). **Ic**,**d** present good second harmonic generation (SHG) properties. UV/Vis spectral investigation indicates that **Ia–d** and **IIa**,**b** are wide-band-gap semiconductors.

Keywords: aluminum · borates · cations · porous materials · transition metals

Introduction

Borates have been a subject of interest for many decades, an interest that is motivated by their rich structural chemistry and potential applications in mineralogy, semiconductor, luminescence, and nonlinear optical properties.[1] Boron is a unique element that reveals two kinds of coordination modes: either BO_3 triangular or BO_4 tetrahedral geometries. Both BO_3 and BO_4 groups favor polymerization through sharing corners into a wide range of large B–O clusters.[2] These polyanionic clusters can be considered as the secondary building units (SBUs) to take part in the construction of novel borates. As expected, a large number of novel 1D, 2D, and 3D extended structures based on the B–O cluster units have been reported, as exemplified by 1D stepped chain constructed out of $B_3O_5(OH)_2^{3-}$ and $B_4O_9^{6-}$ clusters,[3] a 2D noncentrosymmetric layer based on a $[B_5O_{10}(OH)]$ cluster,[4] and a 3D polyborate framework built up from 1D chains of B_4O_9 clusters linked by additional BO_3 groups.[5] It was noteworthy that even though there are a considerable number of theoretically possible fundamental cluster units, only a few are realized in pure borate structures. To enrich the conformation and connection mode of cluster units, some groups attempted to introduce PO_4 tetrahedra into a B–O anionic framework, thus leading to the large group of borophosphates with new condensation patterns of complex anions. As a result, some novel borophosphates with unusual properties have been reported to date and now constitute the largest subclass of the heteroborate family.[6] In contrast, the borates that contain other main group atoms (such as Al,[7] Ga,[8] and Ge[9]) in their frameworks have been less explored under mild hydro(solvo)thermal conditions.

As it is in the same group as B, Al also exhibits a flexible coordination behavior (tetrahedral AlO_4, trigonal-bipyramidal or square-pyramidal AlO_5, and octahedral AlO_6).[10] Since the discovery of Al in aluminosilicate zeolites, Al has been used in making numerous artificial zeolites that possess properties like catalysis, absorption, ion exchange, and

[a] Dr. J. Zhou, W.-H. Fang, Dr. C. Rong, Prof. Dr. G.-Y. Yang
State Key Laboratory of Structural Chemistry
Fujian Institute of Research on the Structure of Matter
Chinese Academy of Sciences, Fuzhou, Fujian 350002 (China)
Fax: (+86) 591-83710051
E-mail: ygy@fjirsm.ac.cn

[b] Prof. Dr. G.-Y. Yang
Department of Chemistry, Beijing Institute of Technology
Beijing 100081 (China)
E-mail: ygy@bit.edu.cn

[c] Dr. J. Zhou
Department of Chemistry and Biology
Yulin Normal University, Yulin, Guangxi 537000 (China)

Supporting information for this article is available on the WWW under http://dx.doi.org/10.1002/chem.200902664.

others.[11] Besides being used in making zeolites, the incorporation of Al into the borate would likely result in a new class of materials with novel topologies and useful properties. However, only limited aluminoborates (ABOs) and aluminum borate chlorides have been reported to date because of the difficulty in growing crystals suitable for structure determination.[7,12] More recently, we have successfully made a series of ABOs by using hydrothermal methods.[13] In these ABOs, the various shapes, sizes, and charges of protonated organic amines or inorganic cations have a significant structure-directing effect on the formation of the 3D ABO anionic frameworks.

Recently, there has been considerable interest in the use of racemic mixtures or optically pure chiral metal complexes (CMCs) as templates instead of organic amines or inorganic cations in making open-framework materials, because the CMCs not only have unique spatial configurations, various charges, different flexibilities, and hydrogen-bonding sites, which lead to the formation of a variety of unusual architectures, but can also imprint their chiral characters into the inorganic host by hydrogen-bonding interactions.[14] In employing CMCs as the templates, a number of metal phosphates and germanates have been made, as exemplified by gallium phosphates,[15] zincophosphates,[14c,16] aluminophosphates,[17] borophosphates,[18] zinc germanates,[19] and nickel germanates.[14e] However, little attention has been paid to the possibility of using CMCs as templates in making ABOs; the only example to our knowledge is 2D ABO $[Zn(dien)_2][\{Al(OH)\}(B_5O_9F)]$ (dien = diethylenetriamine), reported recently by our group.[20] To further investigate the influence of CMCs on the structures of ABOs, we have carried out the synthesis using the mixture of $Al(i\mathrm{PrO})_3/H_3BO_3/M^{2+}$ (or M powder)/amine (M = Co/Ni/Zn/Cd; amine = ethylenediamine (en)/dien) under solvothermal conditions, and obtained two structural types of 3D open-framework ABOs: $[M(dien)_2]\{Al(B_5O_9)[BO_2(OH)]\}$ (M = Co (**Ia**), Ni (**Ib**), Cd (**Ic**), Zn (**Id**)) and $[M(en)_3][AlB_7O_{12}(OH)_2]\cdot(H_2O)_{0.25}$ (M = Co (**IIa**), Ni (**IIb**)) (see Figure 1). Compounds **Ia–d** display a 3D diamond topology based on AlO_4 tetrahedra and $B_6O_{11}(OH)$ clusters as building blocks, whereas **IIa**,**b** exhibit a new 3D framework topology with the total Schläfli symbol of $(4\cdot8^5)(4^3\cdot8\cdot10^2)$ constructed by AlO_4 tetrahedra, chainlike $B_4O_6(OH)_2$ tetramers, and crablike B_6O_{12} clusters. $[M(dien)_2]^{2+}/[M(en)_3]^{2+}$ complex cations reside in the channels of 3D ABO frameworks, which serve as template ions. The present compounds represent the only examples of 3D ABOs templated by TMCs.

Results and Discussion

Synthesis considerations: Hydrothermal methods have been utilized successfully to make a great deal of organic–inorganic hybrid materials, because differential solubilities of organic and inorganic precursors can be overcome.[21] But many factors such as initial reactants, reactant stoichiometry, pressure, pH value, reaction time, and temperature can influence the outcome of hydro(solvo)thermal reactions. For instance, 2D ABO $[Zn(dien)_2][\{Al(OH)\}(B_5O_9F)]$ (**III**) was made by the solvothermal reaction of H_3BO_3, $Al(i\mathrm{PrO})_3$, Zn powder, dien, and H_2O in the presence of HF at 180 °C for 7 days.[20] In **III**, the F^- ion incorporated into the final structure acts as terminating group to prevent further connections to the structural unit. For the aim of preparing of high-dimensional ABOs, the above reaction system was reacted in the absence of HF, and a series of 3D ABOs (**Ia–d**) was successfully obtained. Subsequently, to investigate the influence of different complex cations on the structural construction of the products, the synthetic procedure used for making **Ia–d** was modified: replacing dien with en under similar hydrothermal conditions resulted in the formation of another type of 3D ABOs (**IIa**,**b**). In **Ia–d** and **IIa**,**b**, the different $[M(amine)_x]^{2+}$ complexes formed in situ have a significant templating effect on the formation of two types of 3D ABO anionic frameworks.

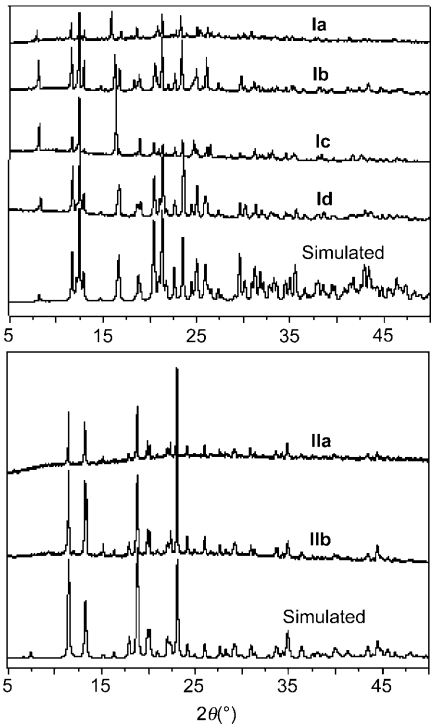

Figure 1. Simulated and experimental powder XRD patterns of **Ia–d** and **IIa**,**b**.

We have studied the influence of synthetic parameters on the obtained compounds: 1) pH: both **Ia–d** and **IIa**,**b** are only obtained in a limited pH domain ($8.0 < pH < 9.2$), if the pH value were higher or lower the expected crystals were not formed. 2) Solvent: the solvent pyridine as a reaction medium is suitable for the crystal growth of the ABOs reported here. Attempts to make both **Ia–d** and **IIa**,**b** with high crystallinity by using other organic solvents such as ethanol, ethylene glycol, and *N*,*N*-dimethylformamide were unsuccessful. 3) Temperature: both **Ia–d** and **IIa**,**b** are only obtained in the range of 170–180 °C. When the reaction temperature was adjusted 10 °C above 180 °C, an amorphous

product was isolated, or 10 °C below 170 °C, only a colloidal product was obtained. 4) Initial reactants: MAc_2 (or $Cd(OH)_2$) or M powder (M = Co, Ni, Zn) is used as the source material, which is very promising for the formation of both **Ia–d** and **IIa**,**b**. Attempts to make both **Ia–d** and **IIa**,**b** by using MX_2 (X = Cl/NO_3) as the M source under similar conditions was fruitless. In addition, Al(*i*PrO)$_3$ rather than traditional Al_2O_3, $AlCl_3$, or $Al(NO_3)_3$ was employed as the Al source, mainly because the Al(*i*PrO)$_3$ is easily dissolved in organic solvents, and the chiral Al center may form from three-coordinated Al(*i*PrO)$_3$ that transforms into a four-coordinated AlO_4 group through the hydrolysis of Al(*i*PrO)$_3$ in the crystallization process, which will greatly increase the likelihood of producing acentric or chiral ABOs.[13] From the systematic exploration of the experimental conditions, the final products of the reaction systems are strongly dependent on pH value, reaction solvent, reaction temperature, and initial reactants. Although no single crystal of compound **Id** suitable for X-ray crystallographic analysis was made, its pure phase has been obtained and determined by X-ray powder diffraction (Figure 1). The result demonstrated that **Id** is isostructural to **Ia–c**. The experimental and simulated powder X-ray diffraction patterns are in good accordance with each other, indicating the phase purity of the sample (Figure 1).

Structure types of 3D ABOs templated by TMCs

Crystals of type I: Compounds **Ia**, **Ib**, **Ic**, and **Id** have the general formula $[M(dien)_2][AlB_6O_{11}(OH)]$ and are isostructural. Therefore, only **Ia** is discussed here in detail. The asymmetric unit of **Ia** consists of one $[AlB_6O_{11}(OH)]^{2-}$ anion and $[Co(dien)_2]^{2+}$ cation (Figure 2a). The $[AlB_6O_{11}(OH)]^{2-}$ anion is composed of one unusual $B_6O_{11}(OH)$ cluster and one typical AlO_4 tetrahedron linked by the common O atom. The $AlB_6O_{11}(OH)$ cluster is constructed by B_5O_{10} unit and $BO_2(OH)$ triangle. The B_5O_{10} cluster is made up of one BO_4 tetrahedron and four BO_3 triangles, in which two B_3O_3 rings are perpendicularly linked by a common BO_4 tetrahedron. The B–O bond lengths vary from 1.318(8) to 1.408(8) Å for the BO_3 triangles and from 1.459(10) to 1.494(10) Å for the BO_4 tetrahedra. The O-B-O bond angles are distributed in the range of 114.6(5)–125.9(6)° for the triangles and 107.4(6)–111.6(5)° for the tetrahedra. The Al–O bond lengths lie in the range of 1.704(4)–1.760(5) Å, and the O-Al-O angles span from 108.7(2) to 112.4(3)°. To determine whether O1 is actually an –OH group, the bond valence sum (BVS) calculations[22] were applied to reveal that the value of the BVS for O1 is −1.08, whereas the other O atoms are in accordance with their formal oxidation state of −2, thereby suggesting that O1 is indeed an OH group. The stoichiometry of $AlB_6O_{11}(OH)$ creates a framework charge of −2, which can be balanced by complex $[Co(dien)_2]^{2+}$ cations.

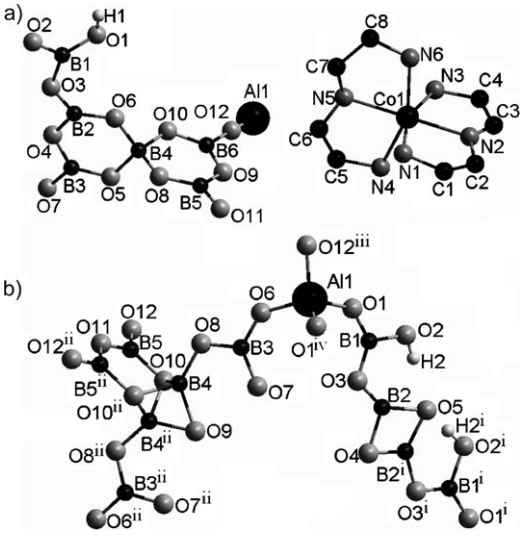

Figure 2. a) The asymmetric unit of **Ia** (hydrogen atoms bonded to C/N atoms have been omitted for clarity). b) The structure of the $[AlB_7O_{12}(OH)_2]^{2-}$ anion in **IIa**. (Symmetry operation: i) $1-x, y, -z$; ii) $1-x, 1-y, z$; iii) $-\frac{1}{2}+x, \frac{1}{2}-y, \frac{1}{2}-z$; iv) x, y, z.)

In **Ia**, each $B_6O_{11}(OH)$ cluster connects 12 others by 4 bridging AlO_4 groups, and each AlO_4 group also links 12 others by means of 4 bridging $B_6O_{11}(OH)$ clusters (Figure 3a). So there is no Al-O-Al connection in the structure. The alternate connectivity between the $B_6O_{11}(OH)$ clusters and the AlO_4 tetrahedra by their vertices gives rise to a novel 3D framework with intersecting channels, two kinds of 1D helical channels with no closed 7- and 9-ring along the [10−1] direction (Figure 3b), arrayed such that each 7-ring channel is surrounded by six 9-ring channels and two 7-ring channels, and vice versa. For the 7-ring helical channel, the unclosed -AlO_4-BO_3-BO_3-AlO_4-BO_3-BO_4-BO_3- linkages give rise to two types of helices with opposite chirality arranged alternately along the [101] direction (Figure 3b and c). The period of the helix is 10.5 Å by the centroid of Al atoms, and the dimension of the helical channel is approximately 5.4 × 6.6 Å^2. The 9-ring helical channel is constructed from the unclosed linkages of -AlO_4-BO_3-BO_3-BO_4-BO_3-AlO_4-BO_3-BO_3-BO_3- and also contains two types of helices with opposite chirality. The left- and right-handed helices are arranged alternately along the [101] direction (Figure 3b and d). The period of the helix is 10.5 Å by the centroid of Al atoms, and the dimension of the helical channel is approximately 6.1 × 8.8 Å^2. The similar 7-ring helical channel is also observed in 2D $[Zn(dien)_2][\{Al(OH)\}(B_5O_9F)]$,[20] but a 9-ring helical channel has not been found in the known 3D ABOs. The 6- or 8-ring helical channel seems to be more frequent.[12b,13]

An important structural feature of **Ia** is that it possesses two types of regular odd 11- and 13-ring channels along the [010] and [100] directions, respectively (Figure 3e–h). Along the [010] direction, the openings of the 11-ring channels are triangular in shape and delimited by two BO_4 tetrahedra, six BO_3 triangles, and three AlO_4 tetrahedra in -AlO_4-BO_3-BO_4-BO_3-AlO_4-BO_3-BO_4-BO_3-AlO_4-BO_3-BO_3- linkages with an approximate free-pore diameter of 8.7 × 10.3 Å (Figure 3e and f; Figure S1a in the Supporting Information).

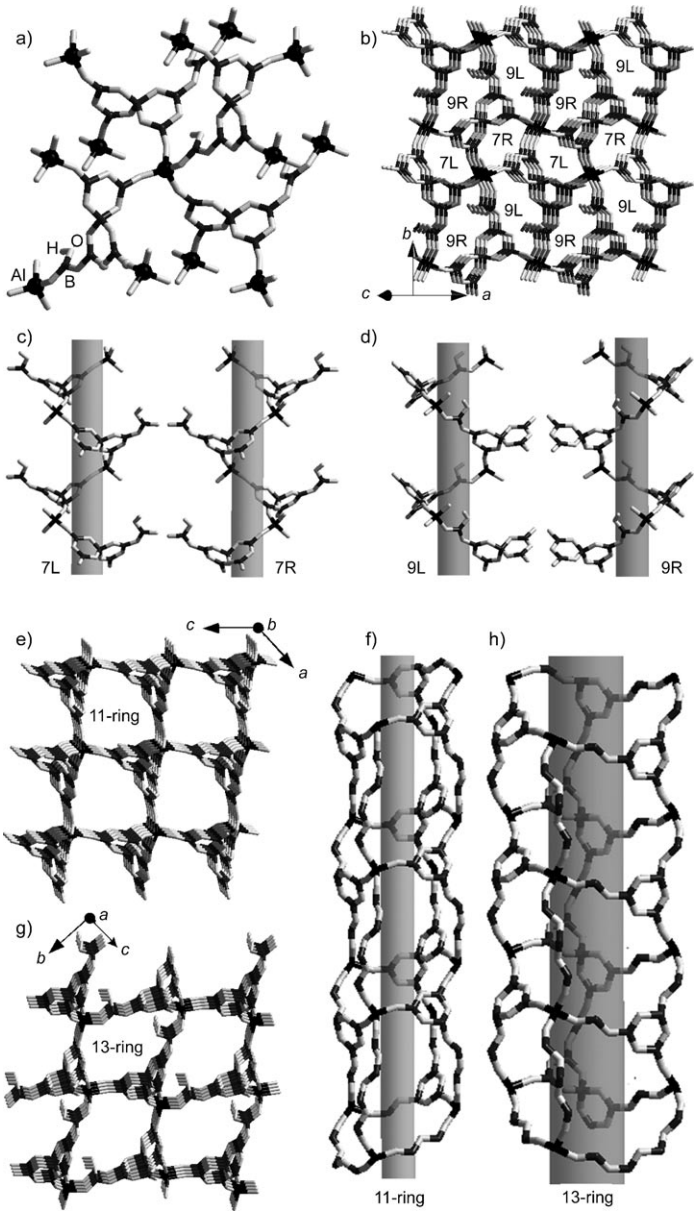

Figure 3. a) View of the linkage of B_5O_{10} clusters and AlO_4 groups in **Ia**. b) View of the 3D framework in **Ia** showing 7- and 9-ring helical channels along the [10−1] direction. c,d) Side view of the left-/right-handed helices. e) View of the 3D framework in **Ia** showing 11-ring channels along the *b* axis. f) The side view of the 11-ring channels. g) View of the 3D framework in **Ia** showing 13-ring channels along the *a* axis. h) Side view of the 13-ring channels.

The pore walls of the 11-ring channels are built from 13-ring windows. Each 11-ring channel is surrounded by 8 neighboring 11-ring channels. Along the [010] direction, the 13-ring channels are elliptical and consist of three AlO_4 tetrahedra, two BO_4 tetrahedra, two $BO_2(OH)$ units, and six BO_3 triangles in -AlO_4-BO_3-BO_4-BO_3-$BO_2(OH)$-AlO_4-BO_3-BO_3-AlO_4-BO_3-BO_4-BO_3-$BO_2(OH)$- linkages with an approximate free-pore diameter of 8.7×11.7 Å (Figure 3g and h; Figure S1b). Their pore walls are built from 11- and 13-ring windows. The $[Co(dien)_2]^{2+}$ cations that reside in the 13-ring channels along the [100] direction (Figure S2) compensate for the negative charge of the polymeric $\{[AlB_6O_{11}(OH)]^{2-}\}_n$ anion framework and interact with the framework O atoms by hydrogen bonding, with N···O distances in the range of 2.994(7)–3.499(8) Å. Similar intermolecular hydrogen bonding is observed in **Ib** and **Ic**.

The $B_6O_{11}(OH)$ cluster based on the linkage of B_5O_{10} cluster and $BO_2(OH)$ group among the known borates is unfamiliar. The analogous framework of pentaborate clusters of $[B_5O_{10-n}(X)_n]^{(5-n)-}$ (X = OH, F; n = 0–4) is commonly observed. These clusters also display different linkages due to the presence of terminal X group. For example, the $B_5O_6(OH)_4^-$ unit (n = 4) has four terminal OH groups and only exists in isolated form because four terminal OH groups prevent the unit further connections.[2c,23] The $B_5O_7(OH)_3^{2-}$ unit (n = 3) acts as a monodentate ligand coordinated to a metal center, thus leading to a neutral molecule.[24] The $B_5O_8(OH)_2^{3-}$ unit (n = 2) as bridging group is directly linked to adjacent ones by means of the *trans*-bridging O atoms to form a 1D chain.[3,25] The $B_5O_9F^{4-}$ unit (n = 1) reported recently by our group acts as three 3-connected nodes to give rise to a 2D layer.[20] The $B_5O_{10}^{5-}$ unit (n = 0) as tetradentate bridging ligand coordinates to four metal centers, thereby generating a 3D open framework.[8,12a,b,13] Although the $B_6O_{11}(OH)$ cluster in **Ia–d** has one terminal OH group, it does not prevent further connections; the $B_6O_{11}(OH)$ cluster also has four potential linking O atoms, similar to four corners of a fictitious $[B_6O_7(OH)]O_4$ tetrahedron. Hence, the $B_6O_{11}(OH)$ cluster exhibits a new type of tetradentate bridging mode.

The structures of **Ia–d** are closely related to those of other ABOs $[Zn(dien)_2][\{Al(OH)\}(B_5O_9F)]$ (**III**),[20] $K_2Al[B_5O_{10}]\cdot 4H_2O$ (**IVa**),[13] $(NH_4)_2Al[B_5O_{10}]\cdot 4H_2O$ (**IVb**),[13] $[CH_3NH_2(CH_2)_3NH_3][AlB_5O_{10}]$ (**IVc**),[12b] $(teta)_2[Al_2B_{10}O_{20}]\cdot 0.25H_2O$ (**Va**, teta = triethylenetetramine),[12a] and $Al[B_5O_{10}]\cdot H_2dab\cdot 2H_2O$ (**Vb**, dab = 1,4-diaminobutane),[13] in which all building blocks contain a B_5O_{10} cluster. Compound **III** might be viewed as a derivative of compounds **Ia–d**. The $B_6O_{11}(OH)$ clusters of **Ia–d** are linked together by AlO_4 tetrahedra to form the 3D framework. However, such connectivity is impossible in **III** because $[BO_2(OH)]$ units of **Ia–d** are replaced by terminal F^- ions (Figure 4a and b). As a result, the 3D framework of **Ia–d** is broken down to 2D layers (Figure S3 in the Supporting Information). So it can be said that the F^- ions act as a "tailor" in the formation of the structure of **III**. The $[BO_2(OH)]$ units of **Ia–d** are also replaced by O atoms to convert into the B_5O_{10} building units of **IVa–c** and **Va–b**. Although both $B_6O_{11}(OH)$ and B_5O_{10} building units can be regarded as the same 4-connected nodes, their linkage modes are different, thus resulting in three types of 3D frameworks. In **IVa–c**, each B_5O_{10} group is linked to 12 other B_5O_{10} groups through 4 bridging AlO_4 units, and each AlO_4 unit is also connected to 12 others by 4 bridging B_5O_{10} groups, thus forming a 3D chiral framework with intersecting helical channels. Although each B_5O_{10}/AlO_4 linkage mode of **Ia–d** is similar to those of **IVa–c**, the odd 13-ring channels of **Ia–d** is obviously larger than those

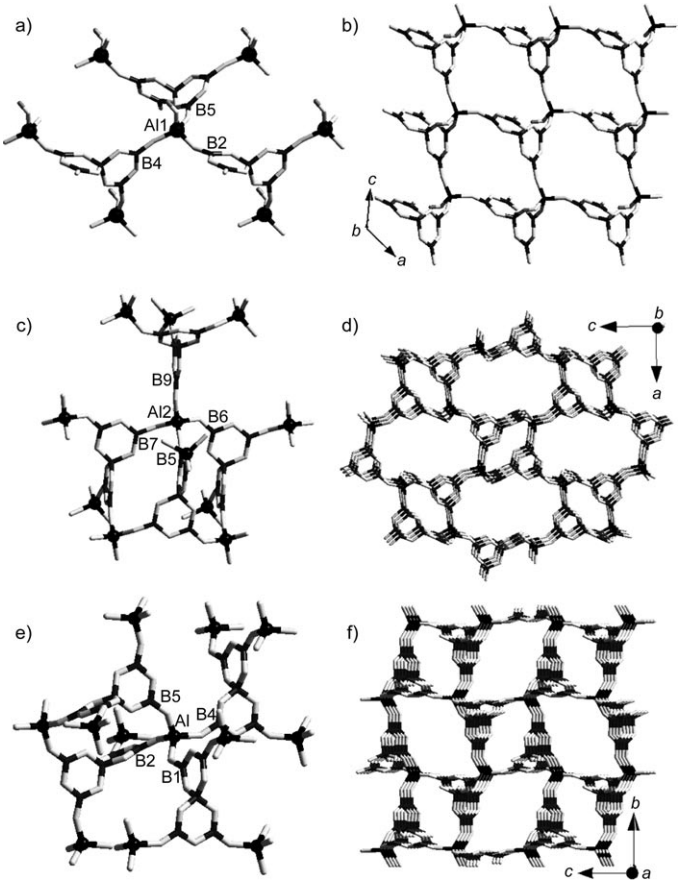

Figure 4. a) View of the linkage of B_5O_9F clusters and $AlO_3(OH)$ groups in **III**. b) View of the 2D layer $[\{Al(OH)\}(B_5O_9F)]_n^{2n-}$ in **III**. c) View of the linkage of B_5O_{10} clusters and AlO_4 groups in **Va**. d) View of a 3D structure of **Va** along the *b* axis. e) View of the linkage of B_5O_{10} clusters and AlO_4 groups in **Vb**. f) The open framework of **Vb** along the *a* axis showing the 12- and 8-ring channels.

of **IVa–c** (11-ring channels). In **Va**, each B_5O_{10}/AlO_4 unit links 10 others by 4 bridging AlO_4/B_5O_{10} units, thereby resulting in a 3D centric framework with 14- and 8-ring elliptical channels along the *b* axis (Figure 4c and d), whereas each B_5O_{10}/AlO_4 unit in **Vb** links 11 others by 4 bridging AlO_4/B_5O_{10} units, thus forming a 3D centric framework with 12- and 8-ring elliptical channels along the *a* axis (Figure 4e and f). Hence, the linkage mode of the $B_6O_{11}(OH)$ cluster in **Ia–d** is significantly different from that of both **IVa–c** and **Va–b**.

From the topological point of view, the 3D frameworks of **Ia–d** have a diamond topology (Figure 5a) in which both $B_6O_{11}(OH)$ clusters and AlO_4 tetrahedra act as 4-connected nodes. Compounds **Ia–d** and **III** all belong to the monoclinic crystal system with space group *Pc*, but they exhibit a different structure. In **III**, the F^- ion substitutes the $BO_2(OH)$ group of the $B_6O_{11}(OH)$ cluster to prevent the structural unit from further connections, thereby resulting in a 2D layer. If the $[B_5O_9F]^{4-}$ clusters can be considered to be 3-connected nodes, the structure of the 2D layer in **III** can be classified as a honeycomb net (hcb) with vertex symbols

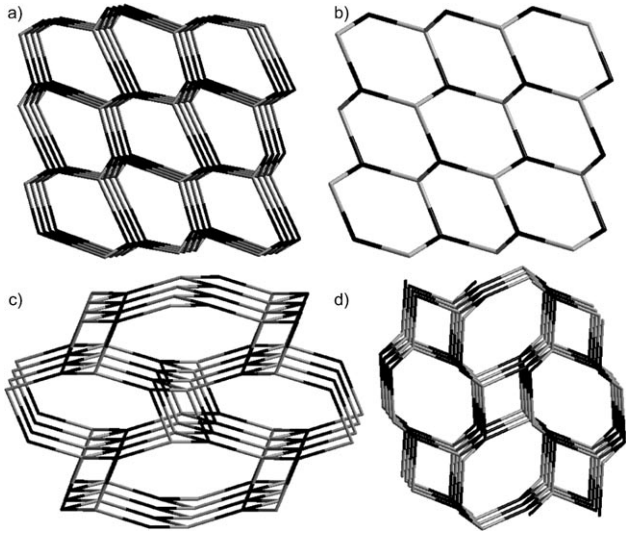

Figure 5. a) The diamond topology of **Ia** with vertex symbols $6_2{\cdot}6_2{\cdot}6_2{\cdot}6_2{\cdot}6_2{\cdot}6_2$. b) The honeycomb net (hcb) of **III** with vertex symbols 6·6·6. c) The ABW topology of **Va** with vertex symbols $4{\cdot}6{\cdot}4{\cdot}6{\cdot}6{\cdot}8_2$. d) The CrB_4 topology of **Vb** with vertex symbols $4{\cdot}6_2{\cdot}6{\cdot}6{\cdot}6{\cdot}6$. Black nodes: B_5O_9X ($X=BO_2(OH)$ (**Ia–d**), F (**III**), O (**Va**,**b**)); gray nodes: AlO_4.

6·6·6 (Figure 5b). The topology framework of **Ia–d** is similar to that of **IVa–c**, but they possess channels of different sizes: **Ia–d** have large 13-ring elliptical channels, whereas **IVa–c** have medium 11-ring elliptical channels. Compounds **Ia–d**, **Va**, and **Vb** have some obvious differences in structure: 1) Different topological types: **Ia–d** have a diamond topology with vertex symbols $6_2{\cdot}6_2{\cdot}6_2{\cdot}6_2{\cdot}6_2{\cdot}6_2$, whereas **Va** has the ABW type of zeolites with vertex symbols $4{\cdot}6{\cdot}4{\cdot}6{\cdot}6{\cdot}8_2$ (Figure 5c) and **Vb** has CrB_4 topology with vertex symbols $4{\cdot}6_2{\cdot}6{\cdot}6{\cdot}6{\cdot}6$ (Figure 5d). 2) Different space groups and sizes of channels: **Ia–d** crystallize in space group *Pc* and have large 13-ring elliptical channels templated by complex $[M(dien)_2]^{2+}$ cations, but **Vb** crystallizes in space group $P2_1/c$ and has large 12-ring elliptical channels templated by inorganic cations (K^+ or NH_4^+); **Va** crystallizes in space group $Pna2_1$ and has large 14-ring elliptical channels templated by teta amine.

Crystal of type II: Compounds $[M(en)_3][AlB_7O_{12}(OH)_2]\cdot(H_2O)_{0.25}$ (M = Co (**IIa**), Ni (**IIb**)) are isostructural and only **IIa** is discussed here in detail. The asymmetric unit of **IIa** contains 0.5 Al atom, 3.5 B atoms, 1 OH group, and 6 O atoms (Figure 2b). There are two types of secondary building unit, namely, the chainlike $B_4O_6(OH)_2$ tetramer and the crablike B_6O_{12} cluster. In the $B_4O_6(OH)_2$ unit, one BO_3 triangle and one $BO_2(OH)$ triangle are joined together by means of sharing an O atom to form a $B_2O_4(OH)$ dimer; two $B_2O_4(OH)$ dimers share a common edge to produce a chainlike $B_4O_6(OH)_2$ tetramer, which possesses an approximately planar B_2O_2 four-membered ring. This tetramer has C_{2v} point symmetry. It is noteworthy that the BO_3 triangles or the combination of BO_3 triangles and BO_4 tetrahedra in the reported borate usually do not share edges, but rather

share corners in a wide range of large B–O clusters.[2–5] So the chainlike $B_4O_6(OH)_2$ tetramer is a rare example of B–O polyhedra sharing edges.

In a crablike B_6O_{12} cluster, two tetrahedral (T) BO_4 are condensed by sharing faces to afford a special B_2O_5 dimer, whereas the linkage of two triangles (Δ) by means of shared corners produces another B_2O_5 dimer. These types of B_2O_5 dimers are further joined together through shared O atoms to give rise to a special tetraborate cluster, B_4O_8, which can be written as $2\Delta+2T$: $<2\Delta T>=<2\Delta T>$ with the help of the conception of fundamental building blocks (FBBs) proposed by Burns et al.[1b,c] This tetraborate cluster is significantly different from the common tetraborate polyanion $[B_4O_5(OH)_4]^{2-}$ ($2\Delta+2T$: $<\Delta 2T>=<\Delta 2T>$).[2a,9c,26] In the $<2\Delta T>=<2\Delta T>$ cluster, there are two nonplanar B_3O_3 rings; the dihedral angle between the planes O12/B5/O11/B5^{ii}/O12^{ii}/O10/O10^{ii} and O10/B4/O10^{ii} is 52.2° (symmetry operation: $-^1/_2+x$, $^1/_2-y$, $^1/_2-z$). The $<2\Delta T>=<2\Delta T>$ cluster can be described as a crab's body. The remaining two BO_3 triangles (2Δ) are similar to the anterior pair of large pincers linked to the crab's body through shared corners to form an unusual crablike hexaborate B_6O_{12} {6:[(4:2Δ+2T)+2(1:Δ)]} that differs from other hexaborate clusters B_6O_{13} [(6:3Δ+3T)][2a,27] and B_6O_{13} {6:2[(3:2Δ+T)]}.[2a,28] Of the bridging O atoms, O10 and O10^{ii} atoms are three-coordinated O centers connected to one tetrahedrally coordinated B atom, respectively; the remainder are two-coordinated O centers. Three-coordinate O centers favor not only nonplanar B_2O_2 ring units but also nonplanar B_3O_3 ring units.

The overall 3D anionic framework of **IIa** is built up from strictly alternating chainlike $B_4O_6(OH)_2$ tetramers, AlO_4 tetrahedra, and crablike B_6O_{12} clusters. Each chainlike $B_4O_6(OH)_2$ tetramer joins two others by means of two bridging AlO_4 groups (Figure S4a in the Supporting Information), whereas each B_6O_{12} cluster links four others through four bridging AlO_4 groups (Figure S4b). Each AlO_4 tetrahedron connects eight others by two bridging chainlike $B_4O_6(OH)_2$ tetramers and two bridging crablike B_6O_{12} clusters (Figure S4c), thereby resulting in no Al-O-Al connection in **IIa**. The alternating connection of the crablike B_6O_{12} clusters and AlO_4 tetrahedra through shared corners generates a 2D layer with (4,4)-network topology in the (001) plane (Figure 6a). These layers are stacked along the *c* axis in an -ABA- sequence (Figure 6b) and are further bridged by chainlike $B_4O_6(OH)_2$ tetramers to lead to the formation of the final 3D $\{AlB_7O_{12}(OH)_2^{2-}\}_n$ framework with 3D intersecting channels (Figure 6c). The network topology of the 3D framework can be simplified by considering the AlO_4 tetrahedra to be 4-connected nodes, crablike B_6O_{12} clusters as 4-connected nodes, and chainlike $B_4O_6(OH)_2$ tetramers as linkers. As a result, a previously unknown framework topology with the total Schläfli symbol of $(4\cdot8^5)(4^3\cdot8\cdot10^2)$ and the long vertex symbol of $(4_2\cdot8_2\cdot8_2\cdot8_2\cdot8_2\cdot8_2)(4_2\cdot8_4\cdot4\cdot10_{20}\cdot4\cdot10_{20})$ is formed (Figure 6d).

Interestingly, two different helical channels with 8- and 16-ring openings can be seen along the [100] and [010] directions (Figure 7a and b). Along the [100] direction, the 8-ring

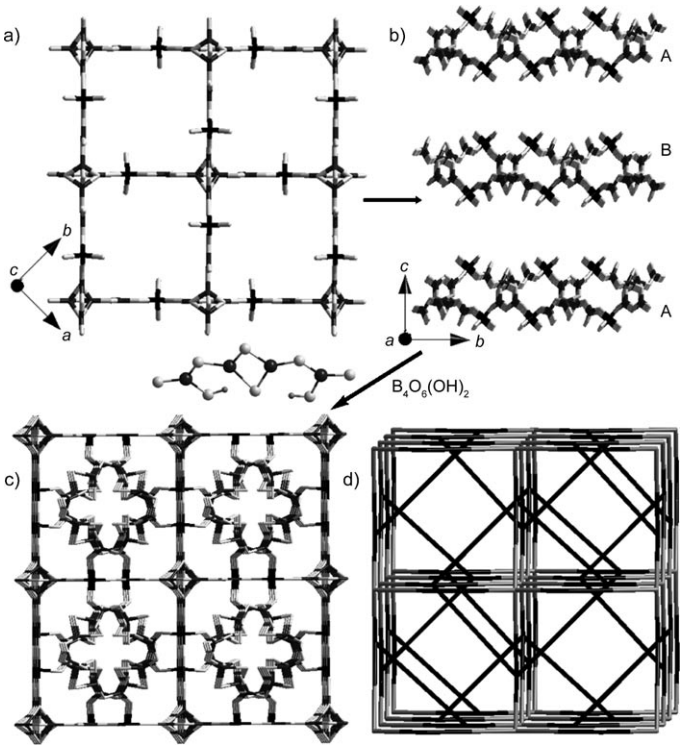

Figure 6. a) 2D layer constructed by the crablike B_6O_{12} clusters and AlO_4 tetrahedra. b) The layers stacked along the *c* axis in an -ABA- sequence. c) 3D network built by 2D layers and chainlike $B_4O_6(OH)_2$ tetramers along the *c* axis. d) The framework topology of **IIa**.

helical channels with right-handedness are rectangular in shape and built from the unclosed linkage of -AlO_4-BO_3-BO_4-BO_3- (Figure 7c). These right helical channels are arranged along the *b* axes. The period of the helix is 13.4 Å by the centroid of Al atoms and the dimension of the helical channel is approximately 8.0×8.6 Å. The 16-ring channel is enclosed by chiral intertwined double helices of the same handedness (left helical, Figure 7d). The helical chains along the 4_2 screw axis are constructed from the connectivity of -AlO_4-BO_2(OH)-BO_3-BO_3-BO_2(OH)-AlO_4-BO_3-BO_3-. The period of the helix is 26.8 Å by the centroid of Al atoms and the dimension of the helical channel is approximately 2.4×10.2 Å^2. Along the [010] direction, similar 8- and 16-ring helical channels can also be observed, but they display reverse handedness: 8-ring left helical channel and 16-ring right helical channel (Figure 7b–d). It is noteworthy that the projection of the double-helical chain units in the (100) or (010) plane resembles the double-helix structure of the DNA; they are different from the reported double-helix chains based on the combination of the right-handed and the left-handed units. Hence, these kinds of double helices with same handedness are particularly rare in inorganic materials. The limited examples include two germanates, $Ge_7O_{12}(OH)_4(C_4N_3H_{13})_{0.5}(H_2O)_5$ and $Ge_7O_{12}(OH)_4(H_2O)_6$,[29] and two phosphates, $[(CH_3)_2NH_2]K_4[V_{10}O_{10}(H_2O)_2(OH)_4(PO_4)_7]_{10}$[30] and $[Zn_2(HPO_4)_4][Co(dien)_2]\cdot H_3O$.[14b] Therefore

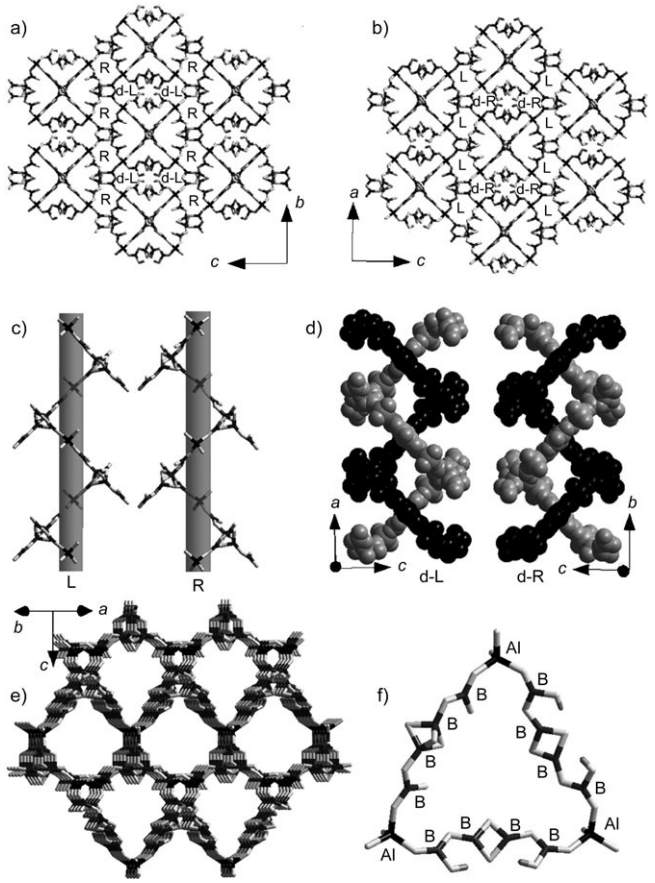

Figure 7. a,b) Framework of **IIa** viewed along the *a*/*b* axis showing 8-/16-ring helical channels. c) L/R indicates the left-/right-handed helical channels, respectively. d) Space-filling diagram of chiral intertwined helices that enclose the 16-ring channel. e) View of the 15-ring channels in **IIa** along the [110] direction. f) Triangular 15-ring opening window in **IIa**.

these 16-ring channels based on same handed units are first encountered in the ABOs.

Besides 8- and 16-ring helical channels, an odd 15-ring channel is observed along the [110] and [1−10] directions (Figure 7e, Figure S5 in the Supporting Information). The opening of the 15-ring channel is triangular in shape and delimited by two BO_4, six BO_3 triangles, four $BO_2(OH)$ units, and three AlO_4 tetrahedra with an approximate diameter of 9.5×11.2 Å^2 (Figure 7f). The odd ring channel is rare among the known crystallized porous materials, with the exception of the 5-ring channel.[31] Until now, the number of odd rings has not exceeded 11 and has only been observed in ICMM6,[32] XA-1,[8] and reported ABOs.[12a,13] Compounds **Ia–d** also display larger odd 13-ring channel. Hence, compounds **IIa–b** represent the first examples of ABO materials with the largest odd 15-ring channels. The $[Co(en)_3]^{2+}$ cations, which reside in 15-ring channels, compensate for the negative charge of the polymeric $\{AlB_7O_{12}(OH)_2^{2-}\}_n$ anion framework and interact with the framework O atoms by hydrogen bonding, with N···O distances in the range of 3.014(1)–3.052(2) Å. Similar intermolecular hydrogen bonding is found in **IIb**.

Structural influences of complex cations: The chelating organic amines coordinate to metal ions to form metal complexes that can combine hydrophilic with hydrophobic structure-directing/templating effects, namely, its positive charge favors the formation of the charged and generally hydrophilic framework, whereas its hydrophobic carbon backbone group tends to favor the more hydrophobic organic surface on the cation assembly. Such an 'amphiphilic' structure-directing/templating effect may play a role in the formation of various new porous frameworks.[14b,33] Notably, metal complexes as new counterions or structure-directing/templating agents may transfer the unique structural features and physical–chemical properties of metal complexes into the host inorganic frameworks, which also provide complementary properties and synergistic effects. Upon examining the symmetries of the host framework and guest structure-directing/templating agents on the basis of the structures described here, the condensation of framework polyhedra around structure-directing/templating agents is dictated by the molecular symmetries of the latter.

In **Ia–c**, there is one independent $[M(dien)_2]^{2+}$ (M = Co, Ni, Cd) cation in the asymmetric unit. All of these transition-metal ions are coordinated by six N atoms of two dien ligands to form a distorted octahedral environment, which is evidenced by the axial N-M-N angles (157.9(2)–176.6(3)° for **Ia**, 162.0(3)–176.6(4)° for **Ib**, and 148.9(3)–172.4(3)° for **Ic**) deviating from 180°. The M−N distances of Co−N (2.117(7)–2.207(6) Å), Ni−N (2.074(7)–2.189(7) Å), and Cd−N (2.326(6)–2.438(9) Å) are similar to the literature values for $[M(dien)_2]^{2+}$ complexes, respectively.[34] The geometric isomers of TMCs with dien ligands have been intensively studied before, and have *s-fac*-, *u-fac*-, and *mer*-configurations,[34d–g] but only the latter two are chiral. In **Ia–c**, there is only chiral *mer*-$[M(dien)_2]^{2+}$ isomer located in the 13-ring channels (Figure 8a and b). The chiral characteristics of the *mer*-$[M(dien)_2]^{2+}$ cations transfer to the ABO framework by N−H···O hydrogen-bond interactions, thus leading to chiral AlO_4 groups and acentric B−O clusters. The combination of chiral AlO_4 groups and acentric B−O clusters results in the acentric characteristic of 3D ABO frameworks.[13]

In **IIa–b**, the asymmetric unit contains a unique transition-metal (M = Co, Ni) center. The N atoms of en ligands bonded to the M center occupy two split positions and have an occupancy of 0.5, which forms the rare trigonal prismatic geometry of the $[M(en)_3]^{2+}$ complex. Each $[M(en)_3]^{2+}$ complex cation itself has two sets of trigonal prismatic geometries that contain three mirror symmetries through M and C1/C2 (or C3/C4) atoms, thus resulting in an achiral enantiomer (Figure S6 in the Supporting Information). The M−N bond lengths are 2.117(7)–2.207(6) Å for Co−N and 2.074(7)–2.189(7) Å for Ni−O, which are consistent with those for $[M(en)_3]^{2+}$ complexes, respectively.[14e,35] Achiral trigonal prismatic $[Co(en)_3]^{2+}$ complexes with two different orientations are alternately arranged in the 15-ring channels along the [110] direction (Figure 8c). The achiral $[Co(en)_3]^{2+}$ complex has C_3 and C_2 symmetry with four mirror planes,

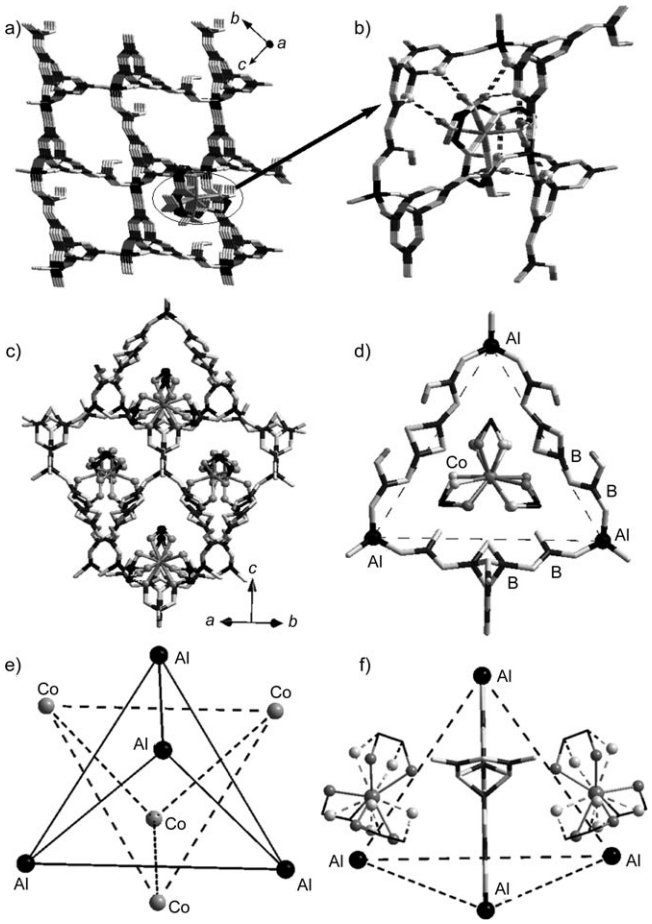

Figure 8. a,b) The $[Co(dien)_2]^{2+}$ cations are located in the 13-ring channels. c,d) $[M(en)_3]^{2+}$ cations located in 15-ring channels. e) Two types of tetrahedra interpenetrate each other. f) One pair of achiral enantiomers.

and the achiral 15-ring motif has C_2 symmetry with one mirror plane. It is appears that the symmetry of the 15-ring motif is a good match with that of the achiral metal-complex templates (Figure 8c). This suggests that the complex template can impose its individual symmetry constraint onto the structural motifs, which have a subgroup of point-group symmetry of the complex template.[14a–c] More interestingly, four AlO_4 tetrahedra are bridged by two crablike B_6O_{12} clusters and four chainlike $B_4O_6(OH)_2$ tetramers to form a supertetrahedral cluster $\{(AlO)_4(B_6O_{12})_2[B_4O_6(OH)_2]_4\}$; each face has an odd 15-ring and four $[Co(en)_3]^{2+}$ cations are located above four respective faces, which constitutes a pseudo tetrahedron (Co_4). Two types of tetrahedra interpenetrate each other (Figure 8e). Four $[Co(en)_3]^{2+}$ cations are divided into two pairs. Each pair has a mirror image relationship, and they are achiral enantiomers (Figure 8f). Although the achiral $[Co(en)_3]^{2+}$ cation in **IIa** displays a templating effect, it does not govern the acentric characteristic of the ABO framework by hydrogen-bonding interactions. This result could be due to the chiral AlO_4 groups in **IIa**,**b** connected by covalent Al-O-B bonds that further transmit their acentric characteristic to the ABO frameworks by the stronger Al-O-B covalent interactions.

Generally, two factors, including the chiral complex cations and the chiral/acentric inorganic groups, will impact the chirality and acentricity of the inorganic frameworks. According to the principle of the host–guest symmetry matching, the chiral complex cations impart their chirality into the host inorganic frameworks. In **Ia–c**, chiral $[M(dien)_2]^{2+}$ cations show strong templating effects and chirality characteristic of $[M(dien)_2]^{2+}$ cations transferred to the ABO frameworks by means of hydrogen-bond interactions, which govern the acentricity of the overall 3D anionic ABO frameworks. Compared with chiral $[M(dien)_2]^{2+}$ cations in **Ia–c**, achiral $[M(en)_3]^{2+}$ cations show weak templating effects and do not govern the acentric characteristic of the framework of **IIa**,**b**. A similar phenomenon has also been observed in $[Al(B_4O_9)(BO)]\cdot H_2en$,[13] in which the centrosymmetric en as a structure-directing agent (SDA) does not govern the acentric characteristic of the ABO framework. Therefore the chirality of complex cations as SDAs is only one of the important factors in making chiral/acentric materials. As to chiral AlO_4 groups and acentric B–O clusters, they not only transfer their chiral/acentric characteristic to inorganic frameworks, they also govern the chiral/acentric characteristic of the ABO frameworks in **IIa–b**.

IR, nonlinear optical (NLO), UV/Vis, and fluorescence spectra: In IR spectra (Figure S7 in the Supporting Information), the broad bands at $\tilde{\nu}=3490$–$3450\ cm^{-1}$ can be attributed to O–H stretching. The stretching bands of $-NH_2$ and $-CH_2$ groups are observed at $\tilde{\nu}=3350$–3180 and 2940–2870 cm^{-1}, respectively, and the asymmetric vibration bands of $-NH_2$ and $-CH_2$ groups also appear at $\tilde{\nu}=1620$–$1600\ cm^{-1}$, respectively. The occurrence of these resonance signals confirms the presence of amino groups in **Ia–d** and **IIa–b**. The vibration absorption region of 1400–1200 cm^{-1} is due to B–O asymmetric bond stretching of BO_3 units, whereas that of BO_4 units appears in the range 1160–1010 cm^{-1}.[2–5] The presence of an absorption peak in the 910–710 cm^{-1} range originates from the vibration of AlO_4 units.[13,20,36]

To consider the noncentrosymmetric structures of **Ia–d** and **IIa**,**b**, second harmonic generation (SHG) measurements were carried out on the powder samples of these compounds by the Kurtz–Perry method at room temperature.[37] The intensity of the green light (frequency-doubled output: $\lambda=532$ nm) produced by the crystal powder of these compounds exhibits an SHG efficiency approximately 0.2 (**Ib**), 1.7 (**Ic**), 1.3 (**Id**), and 0.2 (**IIb**) times of that of KDP (KH_2PO_4) powder, respectively, whereas no SHG efficiency was observed for **Ia** and **IIa** in our measurements, which further confirms that the acentric structures are a necessary condition for NLO materials.

UV/Vis absorption spectra of **Ia–d** and **IIa**,**b** (Figure S8 in the Supporting Information) were calculated from the data of diffuse reflectance by using the Kubelka–Munk function.[38] No absorptions for **Ic**,**d** were observed in the visible region. The absorptions in the range from 0.89 (1400 nm) to 0.50 eV (2500 nm) are related to the multiplication or sum

of the vibration of $-NH_3$, $-CH_2$, and $-OH$ groups. The absence of absorption in the region between 0.89 (1400 nm) and 5.39 eV (230 nm) shows that **Ic**,**d** could be used for optical window applications. Compared with **Ic**,**d**, both **Ia**,**b** and **IIa**,**b** show significant absorption in this region with several maxima at 1.25 (991) and 2.51 eV (493 nm) for **Ia**; 1.45 (855), 2.24 (554), and 3.52 eV (352 nm) for **Ib**; 1.43 (867), 2.26 (549), and 3.55 eV (349 nm) for **IIa**; and 1.26 (984) and 2.56 eV (484 nm) for **IIb**, which could be assigned to the d–d transition in $[M(dien)_2]^{2+}$ or $[M(en)_3]^{2+}$ (M = Co, Ni) complex cations and are consistent with the complicated UV/Vis spectra of previously reported molecular Co^{II}/Ni^{II} complexes.[34a,39] The optical band gaps (E_{onset}) obtained by extrapolation of the linear portion of the absorption edges are estimated to be 4.54 for **Ia**, 4.71 for **Ib**, 5.61 for **Ic**, 5.61 for **Id**, 4.56 for **IIa**, and 4.74 eV for **IIb**, which can be assigned to the lowest possible electronic excitation located at the anion. These band gaps are compared with values of other ABOs ($[Al(B_4O_9)(BO)]\cdot H_2en$ (4.11 eV), $[Al(B_4O_9)(BO)]\cdot H_2dap$ (4.23 eV), and $K_2Al[B_5O_{10}]\cdot 4H_2O$ (4.45 eV),[13] and borates β-BaB_2O_4 (6.43 eV) and LiB_3O_5 (7.78 eV),[40] which exhibit the properties of a wide-band-gap semiconductor.

The emission spectra of compounds **Ia–d** and **IIa**,**b** in the solid state were investigated at room temperature under the same situations (Figure S9 in the Supporting Information). Six compounds all exhibit the strong blue fluorescence emission at 492 nm as a result of excitation at 215 nm. Compared with the value of 450 nm reported for 2D ABO $[Zn(dien)_2][\{Al(OH)\}(B_5O_9F)]$[20] (**III**), there is a redshift of emission, which might result from no further polymerization of the 2D polymeric anion in **III**. Although both **Ia–d** and **IIa**,**b** contain different $[M(dien)_2]^{2+}$ or $[M(en)_3]^{2+}$ (M = Co, Ni) cations in their channels, the emission spectra show that they have almost the same emission intensity at 492 nm, which probably means the fluorescence emission of these compounds is not related to the template cations. Similar phenomena have also been observed in other 3D ABOs with different template cations.[13]

Conclusion

Using chiral complex cations $[M(dien)_2]^{2+}$ (M = Co, Ni, Zn, Cd) and achiral complex cations $[M'(en)_3]^{2+}$ (M′ = Co, Ni) as templates, respectively, two novel types of 3D ABOs have been successfully made under hydrothermal conditions. Type **I** is constructed from AlO_4 tetrahedra and $B_6O_{11}(OH)$ clusters and displays a 3D diamond framework with odd 7-, 9-, 11-, and 13-ring intersecting channels. Although a similar framework has also been observed in other ABOs,[13] it only contains moderately odd 11-ring channels, which are filled by smaller organic amine or inorganic template cations. To accommodate larger $[M(dien)_2]^{2+}$ complex cations in **Ia–d**, the common pentaborate B_5O_{10} cluster as building block is converted into a rare $B_6O_{11}(OH)$ cluster with one dangling $BO_2(OH)$ group, thereby resulting in larger odd 13-ring channels. Therefore, among the ABOs, compounds **Ia–d** provide unusual examples of three intersecting odd-ring channels based on a larger 13-ring channel. Although the topology net of type **II** is different from type **I**, the framework of type **II** is built up from the chainlike $B_4O_6(OH)_2$ tetramer and crablike B_6O_{12} cluster units and exhibits a new $(4\cdot8^5)(4^3\cdot8\cdot10^2)$ topology net. Type **II** shows several unique characteristics. 1) Type **II** contains the largest odd 15-ring channel, because the number of odd rings to date has not exceeded 11 in ICMM6,[32] XA-1,[8] and reported ABOs.[13] 2) The 3D framework is constructed of two kinds of unusual B–O clusters; the reported 2D or 3D B–O or ABO framework is generally built up from same B–O cluster unit.[4,5,12a,b,13] 3) It contains double-helix channels with the same handedness, which are different from the reported double-helix channels based on the combination of the right-/left-handed units. Apart from **Ia** and **IIa**, **Ib–d** and **IIb** show SHG efficiency of about 0.2, 1.7, 1.3, and 0.2 times higher than that of KDP. The UV spectral investigation and theoretical calculations indicate they are wide-band-gap semiconductors. **Ia–d** and **IIa**,**b** can emit fluorescence at 492 nm, thus showing they are potential blue-light materials. The successful synthesis of two types of 3D ABOs not only enriches the existing field of porous materials but also opens possibilities for making other novel ABOs by using different complex cation templates under reasonable conditions.

Experimental Section

Materials and methods: All chemicals were used as purchased without purification. Elemental analyses (C, H, and N) were performed using a PE2400 II elemental analyzer. Energy-dispersive X-ray analysis (EDXA) was taken by using a JEOL JSM-6700F field-emission scanning electron microscope. The UV/Vis spectra were recorded at room temperature using a computer-controlled PE Lambda 900 UV/Vis spectrometer equipped with an integrating sphere in the wavelength range of 190–2000 nm. Fluorescence spectral analyses were performed using a Cary Eclips fluorescence spectrometer. The fundamental wavelength was 1064 nm and was generated by a Q-switched Nd:YAG laser. The SHG wavelength was 532 nm. KDP powder was used as a reference. The IR spectra were obtained using an ABB Bomen MB 102 spectrometer in the range of 4000–400 cm^{-1} with pressed KBr pellets. Thermogravimetric analyses (TGA) were performed using a Mettler TGA/SDTA851 thermal analyzer under an air-flow atmosphere with a heating rate of 10 °C min^{-1} in the temperature region of 30–1000 °C.

Syntheses: Syntheses of the compounds were achieved by a hydrothermal technique in a Teflon-lined stainless steel bomb under synthetic reaction conditions that were determined empirically.

$[Co(dien)_2][AlB_6O_{11}(OH)]$ (Ia): A mixture of $Co(CH_3COO)_2\cdot 4H_2O$ (0.150 g, 0.6 mmol), Al(*i*PrO)$_3$ (0.212 g, 1.0 mmol), and H_3BO_3 (0.349 g, 5.6 mmol) was dispersed in a mixture of H_2O (2.0 mL) and pyridine (3.0 mL) and was stirred to a homogeneous gel, then diethylenetriamine (0.7 mL) was added to the gel. The mixture was transferred to a 23 mL Teflon-lined stainless steel bomb at 180 °C for 11 d and then it was cooled to room temperature. The red crystals were washed with distilled water and then dried in air. The yield was about 81 % (based on Al(*i*PrO)$_3$). When $Co(CH_3COO)_2\cdot 4H_2O$ was also replaced by Co powder under the same synthetic conditions, the crystals of **Ia** were also obtained. IR (KBr): $\tilde{\nu}$ = 3452 (m), 3317 (m), 3270 (m), 3184 (m), 2926 (m), 2874 (m), 1607 (w), 1412 (s), 1331 (s), 1210 (vs), 1078 (m), 1032 (m), 939 (m), 893 (m), 830 (m), 767 (m), 692 (m), 583 (m), 514 (m), 491 (m),

416 cm^{-1} (s); elemental analysis calcd (%) for **Ia**: C 17.47, H 4.95, N 15.28; found: C 17.59, H 4.81, N 15.15.

$[Ni(dien)_2][AlB_6O_{11}(OH)]$ (Ib): The purple crystals of **Ib** were made by a similar method used in the synthesis of the crystals of **Ia** except that $Co(CH_3COO)_2{\cdot}4H_2O$ was replaced by $Ni(CH_3COO)_2{\cdot}4H_2O$ (yield 76%, based on $Al(iPrO)_3$) at 180°C for 11 d. IR (KBr): $\tilde{\nu}$ = 3450 (m), 3321 (m), 3273 (m), 3180 (m), 2925 (m), 2870 (m), 1610 (m), 1446 (m), 1335 (m), 1214 (w), 1152 (vw), 1080 (vw), 1025 (w), 932 (w), 908 (w), 835 (w), 768 (w), 688 (m), 651 (m), 616 (m), 518 (m), 492 (m), 420 cm^{-1} (m); elemental analysis calcd (%) for **Ib**: C 17.47, H 4.95, N 15.28; found: C 16.53, H 4.90, N 14.87. Notice that the observed value (16.53%) of the C atoms is slightly lower than its calculated value (17.47%). By calculation, when one formula $[Ni(dien)_2][AlB_6O_{11}(OH)]$ adsorbs 1.5 water molecules from the air to become $[Ni(dien)_2][AlB_6O_{11}(OH)]{\cdot}1.5H_2O$, the calculated and observed values of the C, H, and N atoms are in good accordance with each other (elemental analysis calcd (%) for $[Ni(dien)_2][AlB_6O_{11}(OH)]{\cdot}1.5H_2O$: C 16.64, H 5.20, N 14.56; found: C 16.53, H 4.90, N 14.87), thus indicating that the above calculation is reasonable.

$[Cd(dien)_2][AlB_6O_{11}(OH)]$ (Ic): The colorless block crystals of **Ic** were prepared by a similar method used in the synthesis of the crystals of **Ia** except that $Co(CH_3COO)_2{\cdot}4H_2O$ was replaced by $Cd(OH)_2$ or $Cd(CH_3COO)_2{\cdot}4H_2O$ (yield: 52%, based on $Al(iPrO)_3$) at 180°C for 11 d. IR (KBr): $\tilde{\nu}$ = 3487 (m), 3344 (s), 3278 (s), 2918 (s), 2870 (s), 1605 (s), 1476 (s), 1220 (m), 1030 (w), 897 (w), 823 (w), 767 (w), 719 (m), 669 (m), 622 (m), 585 (m), 492 (m), 426 cm^{-1} (m); elemental analysis calcd (%) for **Ic**: C 15.92, H 4.51, N 13.92; found: C 15.68, H 4.47, N 13.34.

$[Zn(dien)_2][AlB_6O_{11}(OH)]$ (Id): The colorless microcrystals of **Id** were prepared by a similar method used in the synthesis of the crystals of **Ia** except that $Co(CH_3COO)_2{\cdot}4H_2O$ was replaced by $Zn(CH_3COO)_2{\cdot}4H_2O$ (yield: 42%, based on $Al(iPrO)_3$) at 180°C for 11 d. IR (KBr): $\tilde{\nu}$ = 3469 (s), 3321 (s), 3273 (s), 3180 (s), 2918 (s), 2875 (s), 1617 (m), 1470 (m), 1160 (w), 1030 (w), 934 (vw), 903 (w), 842 (w), 768 (w), 720 (m), 591 (w), 500 (w), 420 cm^{-1} (w); elemental analysis calcd (%) for **Id**: C 17.26, H 4.89, N 15.10; found: C 17.15, H 4.98, N 14.97.

$[Co(en)_3][AlB_7O_{12}(OH)_2]{\cdot}(H_2O)_{0.25}$ (IIa): In a typical synthesis for **IIa**, a mixture of $Al(iPrO)_3$ (0.204 g, 1.0 mmol), Co powder (0.059 g, 1.0 mmol), H_3BO_3 (0.376 g, 6.0 mmol), H_2O (1.0 mL), ethylenediamine (0.7 mL), and pyridine (3.0 mL) was reacted in a 30 mL Teflon-lined stainless steel bomb at 180°C for 7 d and then cooled to room temperature. Red block crystals suitable for X-ray diffraction were obtained in 65% yield (based on $Al(iPrO)_3$). IR (KBr): $\tilde{\nu}$ = 3480 (s), 3321 (s), 3273 (s), 2925 (m), 2881 (s), 1617 (m), 1446 (s), 1305 (m), 1207 (w), 1109 (vw), 1011 (m), 921 (m), 852 (w), 817 (m), 768 (vw), 720 (m), 682 (m), 645 (m), 579 (w), 505 (w), 468 cm^{-1} (w); elemental analysis calcd (%) for **IIa**: C 12.59, H 4.63, N 14.69; found: C 12.34, H 4.92, N 14.35.

$[Ni(en)_3][AlB_7O_{12}(OH)_2]{\cdot}(H_2O)_{0.25}$ (IIb): The purple block crystals of **IIb** were prepared by a similar method used in the synthesis of the crystals of **IIa** except that Co powder was replaced by Ni powder (yield: 52%, based on $Al(iPrO)_3$) at 180°C for 11 d. IR (KBr): $\tilde{\nu}$ = 3480 (s), 3334 (s), 3291 (s), 2931 (m), 2881 (s), 1617 (m), 1451 (m), 1396 (m), 1300 (m), 1202 (w), 1104 (w), 1019 (m), 921 (m), 853 (m), 810 (m), 712 (s), 645 (s), 511 (m), 475 cm^{-1} (w); elemental analysis calcd (%) for **IIb**: C 12.60, H 4.63, N 14.69; found: C 12.30, H 4.93, N 14.26.

X-ray crystallography: Intensity data were collected at 293 K using a RIGAKU Mercury CCD diffractometer for **Ia–d** and **IIa**,**b** using graphite-monochromated $Mo_{K\alpha}$ radiation (λ = 0.71073 Å), respectively. All absorption corrections were performed using the multiscan program. The structures were solved by direct methods and refined by full-matrix least-squares methods on F^2 with the SHELXTL-97 program package.[41] All of the non-hydrogen atoms were refined anisotropically. No hydrogen atoms associated with the water molecules were located from the difference Fourier map. The hydrogen atoms for compounds **Ia–c** were positioned with idealized geometry and refined with fixed isotropic displacement parameters, whereas the hydrogen atoms of en ligands for compounds **IIa** and **IIb** were not dealt with due to the disorder of en. For **IIa**,**b**, the O5 atom and all N atoms were disordered over two positions with the occupation factors of 0.5 and 0.5, respectively. The occupation factor of O1W in **IIa**,**b** was determined as 0.25 according to the results of CHN analysis. Crystallographic data and structure refinements for **Ia–c** and **IIa**,**b** are given in Table 1. CCDC-745573 (**Ia**), 745574 (**Ib**), 745575 (**Ic**), 745576 (**IIa**), and 745577 (**IIb**) contain the supplementary crystallographic data for this paper. These data can be obtained free of charge from The Cambridge Crystallographic Data Centre via www.ccdc.cam.ac.uk/data_request/cif.

Table 1. X-ray crystallographic data for **Ia–c** and **IIa**,**b**.

	Ia	**Ib**	**Ic**	**IIa**	**IIb**
formula	$C_8H_{27}AlB_6CoN_6O_{12}$	$C_8H_{27}AlB_6N_6NiO_{12}$	$C_8H_{27}AlB_6CdN_6O_{12}$	$C_6H_{26.5}AlB_7CoN_6O_{14.25}$	$C_6H_{26.5}AlB_7N_6NiO_{14.25}$
M_r	550.13	549.89	603.61	572.22	571.98
crystal system	monoclinic	monoclinic	monoclinic	tetragonal	tetragonal
space group	*Pc*	*Pc*	*Pc*	$I\bar{4}2m$	$I\bar{4}2m$
a [Å]	9.1836(18)	9.3463(19)	9.4602(19)	13.3906(19)	13.3944(19)
b [Å]	11.161(2)	10.919(2)	10.765(2)	13.3906(19)	13.3944(19)
c [Å]	13.702(4)	13.776(4)	13.816(4)	26.573(5)	26.498(5)
β [°]	130.239(19)	129.880(19)	129.657(19)	90	90
V [$Å^3$]	1072.1(5)	1078.8(4)	1083.2(4)	4764.8(13)	4754.0(13)
Z	2	2	2	8	8
T [K]	293(2)	293(2)	293(2)	293(2)	293(2)
ρ_{calcd} [$g\,cm^{-3}$]	1.704	1.693	1.851	1.527	1.530
μ [mm^{-1}]	0.913	1.011	1.120	0.804	0.892
F(000)	566	568	608	1608	1544
2θ (max) [°]	54.96	54.92	54.96	50.18	50.12
reflns collected	7834	8338	8310	15200	14922
unique reflns	4497	3434	4030	2235	2206
no. of parameters	308	308	307	219	219
R_1[a] ($I>2\sigma(I)$)	0.0591	0.0625	0.0470	0.0798	0.0748
wR_2[b] ($I>2\sigma(I)$)	0.1498	0.1271	0.1141	0.2170	0.2038
R_1[a] (all data)	0.0712	0.0943	0.0615	0.0843	0.0770
wR_2[b] (all data)	0.1561	0.1433	0.1377	0.2268	0.2076
GOF on F^2	1.011	0.992	1.090	1.074	1.055
peak/hole [e $Å^{-3}$]	1.188/−0.530	0.650/−0.515	0.952/−1.403	0.673/−0.561	0.635/−0.736

[a] $R_1 = \Sigma||F_o|-|F_c||/\Sigma|F_o|$. [b] $wR_2 = \Sigma w(F_o^2-F_c^2)^2/\Sigma w(F_o^2)^2]^{1/2}$; $w = 1/[\sigma^2(F_o^2)+(xP)^2+yP]$; $P = (F_o^2+2F_c^2)/3$, in which x = 0.0902, y = 0 for **Ia**; x = 0.0617, y = 0 for **Ib**; x = 0.0728, y = 0 for **Ic**; x = 0.1668, y = 5.1068 for **IIa**; x = 0.1522, y = 6.9628 for **IIb**.

Acknowledgements

This work was supported by the National Natural Science Fund of China (no. 50872133), the NNSF for Distinguished Young Scholars of China (no. 20725101), the 973 Program (no. 2006CB932904), the Key Project from FJIRSM (no. SZD07001), the NSF of Fujian Province (no. E0510030), the NNSF of China (no. 20821061), and China Postdoctoral Science Foundation (no. 20090450184).

[1] a) P. C. Burns, *Can. Mineral.* **1995**, 33, 1167–1176; b) J. D. Grice, P. C. Burns, F. C. Hawthorne, *Can. Mineral.* **1999**, 37, 731–762; c) P. C. Burns, J. D. Grice, F. C. Hawthorne, *Can. Mineral.* **1995**, 33, 1131–1151; d) C. Chen, Y. Wang, B. Wu, K. Wu, W. Zeng, L. Yu, *Nature* **1995**, *373*, 322–324; e) P. Becker, *Adv. Mater.* **1998**, *10*, 979–992; f) M.-S. Wang, G.-C. Guo, W.-T. Chen, G. Xu, W.-W. Zhou, K.-J. Wu, J.-S. Huang, *Angew. Chem.* **2007**, *119*, 3983–3985; *Angew. Chem. Int. Ed.* **2007**, *46*, 3909–3911; g) S. Pan, J. P. Smit, B. Watkins, M. R. Marvel, C. L. Stern, K. R. Poeppelmeier, *J. Am. Chem. Soc.* **2006**, *128*, 11631–11634; h) F. Kong, S.-P. Huang, Z.-M. Sun, J.-G. Mao, W.-D. Cheng, *J. Am. Chem. Soc.* **2006**, *128*, 7750–7751.

[2] a) M. Touboul, N. Penin, G. Nowogrocki, *Solid State Sci.* **2003**, *5*, 1327–1342; b) Z.-H. Liu, L.-Q. Li, *Cryst. Growth Des.* **2006**, *6*, 1247–1249; c) M. Z. Visi, C. B. Knobler, J. J. Owen, M. I. Khan, D. M. Schuber, *Cryst. Growth Des.* **2006**, *6*, 538–545; d) C.-Y. Pan, G.-M. Wang, S.-T. Zheng, G.-Y. Yang, *Z. Anorg. Allg. Chem.* **2007**, 633, 336–340; e) D. M. Schubert, M. Z. Visi, S. Khan, C. B. Knobler, *Inorg. Chem.* **2008**, *47*, 4740–4745; f) D. M. Schubert, M. Z. Visi, C. B. Knobler, *Inorg. Chem.* **2000**, *39*, 2250–2251; g) Z.-H. Liu, L.-Q. Li, W.-J. Zhang, *Inorg. Chem.* **2006**, *45*, 1430–1432.

[3] H.-X. Zhang, J. Zhang, S.-T. Zheng, G.-Y. Yang, *Cryst. Growth Des.* **2005**, *5*, 157–161.

[4] S. Yang, G. Li, S. Tian, F. Liao, J. Lin, *Cryst. Growth Des.* **2007**, *7*, 1246–1250.

[5] P. Lu, Y. Wang, J. Lin, L. You, *Chem. Commun.* **2001**, 1178–1179.

[6] a) S. C. Sevov, *Angew. Chem.* **1996**, *108*, 2814–2816; *Angew. Chem. Int. Ed. Engl.* **1996**, *35*, 2630–2632; b) R. P. Bontchev, J. Do, A. J. Jacobson, *Angew. Chem.* **1999**, *111*, 2063–2066; *Angew. Chem. Int. Ed.* **1999**, *38*, 1937–1940; c) G. Schäfer, W. Carrillo-Cabrera, S. Leoni, H. Borrmann, R. Kniep, *Z. Anorg. Allg. Chem.* **2002**, *628*, 67–76; d) Y.-X. Huang, G. Schäfer, W. Carrillo-Cabrera, H. Borrmann, R. Cardoso Gil, R. Kniep, *Chem. Mater.* **2003**, *15*, 4930–4935; e) R. Kniep, H. G. Will, I. Boy, C. Röhr, *Angew. Chem.* **1997**, *109*, 1052–1054; *Angew. Chem. Int. Ed. Engl.* **1997**, *36*, 1013–1014; f) I. Boy, F. Stowasser, G. Schäfer, R. Kniep, *Chem. Eur. J.* **2001**, *7*, 834–839; g) W. Liu, M. Ge, X. Yang, H. Chen, M. Li, J. Zhao, *Inorg. Chem.* **2004**, *43*, 3910–3914; h) P. W. Menezes, S. Hoffmann, Y. Prots, R. Kniep, *Inorg. Chem.* **2007**, *46*, 7503–7508.

[7] a) J. Ju, J. Lin, G. Li, T. Yang, H. Li, F. Liao, C.-K. Loong, L. You, *Angew. Chem.* **2003**, *115*, 5765–5768; *Angew. Chem. Int. Ed.* **2003**, *42*, 5607–5610; b) J. Ju, T. Yang, G. Li, F. Liao, Y. Wang, L. You, J. Lin, *Chem. Eur. J.* **2004**, *10*, 3901–3906; c) T. Yang, J. Ju, G. Li, F. Liao, X. Zou, F. Deng, L. Chen, Y. Wang, J. Lin, *Inorg. Chem.* **2007**, *46*, 4772–4774; d) T. Yang, J. Sun, L. Eriksson, G. Li, X. Zou, F. Liao, J. Lin, *Inorg. Chem.* **2008**, *47*, 3228–3233.

[8] Z.-H. Liu, P. Yang, P. Li, *Inorg. Chem.* **2007**, *46*, 2965–2967.

[9] a) M. S. Dadachov, K. Sun, T. Conradsson, X. Zou, *Angew. Chem.* **2000**, *112*, 3820–3822; *Angew. Chem. Int. Ed.* **2000**, *39*, 3674–3676; b) D.-B. Xiong, J.-T. Zhao, H.-H. Chen, X.-X. Yang, *Chem. Eur. J.* **2007**, *13*, 9862–9865; c) C.-Y. Pan, G.-Z. Liu, S.-T. Zheng, G.-Y. Yang, *Chem. Eur. J.* **2008**, *14*, 5057–5063; d) H.-X. Zhang, J. Zhang, S.-T. Zheng, G.-M. Wang, G.-Y. Yang, *Inorg. Chem.* **2004**, *43*, 6148–6150; e) H.-X. Zhang, J. Zhang, S.-T. Zheng, G.-Y. Yang, *Inorg. Chem.* **2005**, *44*, 1166–1168.

[10] a) W. H. Casey, M. M. Olmstead, B. L. Phillips, *Inorg. Chem.* **2005**, *44*, 4888–4890; b) L. Allouche, C. Gérardin, T. Loiseau, G. Férey, F. Taulelle, *Angew. Chem.* **2000**, *112*, 521–524; *Angew. Chem. Int. Ed.* **2000**, *39*, 511–514; c) K. Wang, J. Yu, P. Miao, Y. Song, J. Li, Z. Shi, R. Xu, *J. Mater. Chem.* **2001**, *11*, 1898–1902; d) L. M. Meyer, R. C. Haushalter, *Chem. Mater.* **1994**, *6*, 349–350.

[11] C. Baerlocher, W. M. Meier, D. H. Olson, *Atlas of Zeolite Framework Types*, Elsevier, Amsterdam, **2001**.

[12] a) G.-M. Wang, J.-H. Li, Z.-X. Li, H.-L. Huang, S.-Y. Xue, H.-L. Liu, *Inorg. Chem.* **2008**, *47*, 1270–1272; b) G.-M. Wang, J.-H. Li, H.-L. Huang, H. Li, J. Zhang, *Inorg. Chem.* **2008**, *47*, 5039–5041; c) S. Yang, G. Li, J. Ju, Z. Yang, F. Liao, Y. Wang, J. Lin, *Inorg. Chim. Acta* **2008**, *361*, 2413–2417.

[13] C. Rong, Z. Yu, Q. Wang, S.-T. Zheng, C.-Y. Pan, F. Deng, G.-Y. Yang, *Inorg. Chem.* **2009**, *48*, 3650–3659.

[14] a) K. Morgan, G. Gainsford, N. Milestone, *J. Chem. Soc. Chem. Commun.* **1995**, 425–426; b) Y. Wang, J. Yu, M. Guo, R. Xu, *Angew. Chem.* **2003**, *115*, 4223–4226; *Angew. Chem. Int. Ed.* **2003**, *42*, 4089–4092; c) Y. Wang, J. Yu, Y. Li, Z. Shi, R. Xu, *Chem. Eur. J.* **2003**, *9*, 5048–5055; d) H.-X. Zhang, J. Zhang, S.-T. Zheng, G.-Y. Yang, *Inorg. Chem.* **2003**, *42*, 6595–6597; e) Z.-E. Lin, J. Zhang, J.-T. Zhao, S.-T. Zheng, C.-Y. Pan, G.-M. Wang, G.-Y. Yang, *Angew. Chem.* **2005**, *117*, 7041–7044; *Angew. Chem. Int. Ed.* **2005**, *44*, 6881–6884.

[15] a) S. M. Stalder, A. P. Wilkinson, *Chem. Mater.* **1997**, *9*, 2168–2173; b) Y. Wang, J. Yu, Z. Shi, R. Xu, *J. Solid State Chem.* **2003**, *170*, 176–181; c) Y. Wang, J. Yu, Y. Du, R. Xu, *J. Solid State Chem.* **2004**, *177*, 2511–2517.

[16] J. Yu, Y. Wang, Z. Shi, R. Xu, *Chem. Mater.* **2001**, *13*, 2972–2978.

[17] a) M. J. Gray, J. D. Jasper, A. P. Wilkinson, *Chem. Mater.* **1997**, *9*, 976–980; b) K. R. Morgan, G. J. Gainsford, N. B. Milestone, *Chem. Commun.* **1997**, 61–62.

[18] G.-Y. Yang, S. C. Sevov, *Inorg. Chem.* **2001**, *40*, 2214–2215.

[19] X. Bu, P. Feng, G. D. Stucky, *Chem. Mater.* **2000**, *12*, 1811–1813.

[20] J. Zhou, S.-T. Zheng, M. Zhang, G.-Z. Liu, G.-Y. Yang, *CrystEngComm* **2009**, 11, 2597–2600.

[21] a) R. L. LaDuca, Jr., R. S. Rarig, Jr., P. J. Zapf, J. Zubieta, *Inorg. Chim. Acta* **1999**, *292*, 131–136; b) C. Pichon, A. Dolbecq, P. Mialane, J. Marrot, E. Rivière, M. Goral, M. Zynek, T. McCormac, S. A. Borshch, E. Zueva, F. Sécheresse, *Chem. Eur. J.* **2008**, *14*, 3189–3199; c) J.-W. Zhao, H.-P. Jia, J. Zhang, S.-T. Zheng, G.-Y. Yang, *Chem. Eur. J.* **2007**, *13*, 10030–10045; d) J.-W. Zhao, C.-M. Wang, J. Zhang, S.-T. Zheng, G.-Y. Yang, *Chem. Eur. J.* **2008**, *14*, 9223–9239; e) C.-M. Liu, D.-Q. Zhang, D.-B. Zhu, *Cryst. Growth Des.* **2003**, *3*, 363–368; f) N. Snejko, M. E. Medina, E. Gutierrez-Puebla, M. A. Monge, *Inorg. Chem.* **2006**, *45*, 1591–1594.

[22] I. D. Brown, D. Altermatt, *Acta Crystallogr. Sect. B* **1985**, *41*, 244–247.

[23] a) H.-X. Yang, W.-J. Zhang, X.-L. Liu, Z.-H. Liu, *Acta Crystallogr. Sect. E* **2006**, *62*, o4877–o4879; b) C.-Y. Pan, G.-M. Wang, S.-T. Zheng, G.-Y. Yang, *Acta Crystallogr. Sect. E* **2007**, *63*, o840–o842; c) W.-J. Zhang, Z.-H. Liu, *Z. Kristallogr. New Cryst. Struct.* **2006**, *221*,189–190.

[24] a) G.-M. Wang, Y.-Q. Sun, G.-Y. Yang, *J. Solid State Chem.* **2005**, *178*, 729–735; b) G.-M. Wang; Y.-Q. Sun, G.-Y. Yang, *J. Solid State Chem.* **2006**, *179*,1545–1553.

[25] G.-M. Wang, J.-H. Li, Z.-X. Li, P. Wang, H. Li, *Z. Anorg. Allg. Chem.* **2008**, 634, 1192–1196.

[26] a) G.-M. Wang, Y.-Q. Sun, G.-Y. Yang, *J. Solid State Chem.* **2004**, *177*, 4648–4654; b) T. J. R. Weakley, *Acta Crystallogr. Sect. C* **1985**, *41*, 377–379.

[27] a) Z. Liu, L. Li, J. Li, M. Hu, *J. Alloys Compd.* **2005**, *394*, 277–281; b) S. Natarajan, W. Klein, M. Panthöfer, L. Wüllen, M. Jansen, *Z. Anorg. Allg. Chem.* **2003**, *629*, 959–962.

[28] M. Li, J. Chang, Z. Wang, H. Shi, *J. Solid State Chem.* **2006**, *179*, 3265–3269.

[29] Y. Xu, L. Cheng, W. You, *Inorg. Chem.* **2006**, *45*, 7705–7708.

[30] V. Soghomonian, Q. Chen, R. C. Haushalter, J. Zubieta, C. J. O'Connor, *Science* **1993**, *259*, 1596–1599.

[31] Z.-E. Lin, J. Zhang, G.-Y. Yang, *Inorg. Chem.* **2003**, *42*, 1797–1799.

[32] M. E. Medina, M. Iglesias, N. Snejko, E. Gutiérrez-Puebla, M. A. Monge, *Chem. Mater.* **2004**, *16*, 594–599.

[33] a) P. Vaqueiro, *Inorg. Chem.* **2006**, *45*, 4150–4156; b) P. Vaqueiro, A. M. Chippindale, A. V. Powell, *Inorg. Chem.* **2004**, *43*, 7963–7965; c) A. V. Powell, R. J. E. Lees, A. M. Chippindale, *Inorg. Chem.* **2006**, *45*, 4261–4267.

[34] a) J. Zhou, G.-Q. Bian, Y. Zhang, Q.-Y. Zhu, C.-Y. Li, J. Dai, *Inorg. Chem.* **2007**, *46*, 6347–6352; b) D. X. Jia, Y. Zhang, Q. X. Zhao, J. Deng, *Inorg. Chem.* **2006**, *45*, 9812–9817; c) S.-T. Zheng, J. Zhang, G.-Y. Yang, *Inorg. Chem.* **2005**, *44*, 2426–2430; d) R. Stähler, C. Näther, W. Bensch, *J. Solid State Chem.* **2003**, *174*, 264–275; e) R. Stähler, W. Bensch, *Z. Anorg. Allg. Chem.* **2002**, 628, 1657–1662; f) F. R. Keene, G. H. Searle, *Inorg. Chem.* **1974**, *13*, 2173–2180; g) F. R. Keene, G. H. Searle, *Chem. Commun.* **1970**, 784–786.

[35] J. Zhou, Y. Zhang, G.-Q. Bian, Q.-Y. Zhu, C.-Y. Li, J. Dai, *Cryst. Growth Des.* **2007**, *7*, 1889–1892.

[36] H. S. Song, J. Zhang, J. Lin, S. J. Liu, J. J. Luo, Y. Huang, E. M. Elssfah, A. Elsanousi, X. X. Ding, J. M. Gao, C. Tang, *J. Phys. Chem. C* **2007**, *111*, 1136–1139.

[37] S. K. Kurtz, T. T. Perry, *J. Appl. Phys.* **1968**, *39*, 3798–3813.

[38] W. W. Wendlandt, H. G. Hecht, *Reflectance Spectroscopy*, Wiley-Interscience, New York, **1966**.

[39] a) C. Zimmermann, C. E. Anson, F. Weigend, R. Clérac, S. Dehnen, *Inorg. Chem.* **2005**, *44*, 5686–5695; b) B. Kersting, D. Siebert, D. Volkmer, M. J. Kolm, C. Janiak, *Inorg. Chem.* **1999**, *38*, 3871–3882; c) R. Mattes, C. Mühlenbrock, K. Leeners, C. Pyttel, *Z. Anorg. Allg. Chem.* **2004**, *630*, 722–729.

[40] R. H. French, J. W. Ling, F. S. Ohuchi, C. T. Chen, *Phys. Rev. B* **1991**, *44*, 8496–8502.

[41] G. M. Sheldrick, *Acta Crystallogr.* **2008**, *A64*, 112–122: a) SHELXS97, Program for Crystal Structure Solution, G. M. Sheldrick, University of Göttingen, Göttingen, **1997**; b) SHELXL97, Program for Crystal Structure Refinement, G. M. Sheldrick, University of Göttingen, Göttingen, **1997**.

Received: September 28, 2009
Published online: March 22, 2010

